Generalized kekulenes and clarenes as novel families of cycloarenes: structures, stability, and spectroscopic properties

Ke Du and Yang Wang*

School of Chemistry and Chemical Engineering, Yangzhou University, Yangzhou, Jiangsu 225002, China

E-mail: yangwang@yzu.edu.cn

Abstract

Cycloarenes constitute a captivating class of polycyclic aromatic hydrocarbons with unique structures and properties, but their synthesis represents a challenging task in organic chemistry. Kekulene and edge-extended kekulenes as a classic type of cycloarene play an important role in the comprehension of π electron distribution, but the sparse molecular diversity considerably limits their further development and application. In this work, we propose two novel classes of cycloarenes, the generalized kekulenes and the clarenes. Using density functional theory, we carry out a comprehensive study of all possible isomers of the generalized kekulenes and clarenes with different sizes. By applying a simple Hückel model, we show that π delocalization plays a crucial role in determining the relative stability of isomers. We also discover that π-π stacking is commonly present in certain larger clarenes and provides a considerable additional stabilization effect, making the corresponding isomers the lowest-energy ones. Among all considered typical looped polyarenes, generalized kekulenes and/or clarenes are revealed to be the energetically most stable forms, suggesting that these novel cycloarenes proposed here would be viable targets for future synthetic work. The simulated ^{1}H NMR spectra and UV-vis absorption spectra provide valuable information about the electronic and optoelectronic properties for the most stable generalized kekulene and clarene species and may support their identification in future synthesis and experimental characterization.

1 Introduction

Cycloarenes are a class of fully fused macrocyclic aromatic hydrocarbons comprising angular and linear annellations of benzene units enclosing a cavity into which C-H bonds point.[1] Due to their remarkable properties and potential applications in optoelectronics,[2,3] synthetic chemistry,[4–6] supramolecular chemistry,[7,8] etc., cycloarenes have attracted the scientific community for decades.[5] In addition, the large cavity structure offers cycloarenes some promising applications in host-guest chemistry. Cycloarenes can act as a receptor for small guests and have the ability to bind chloride anions due to the large cavity.[8] Moreover, a more modern application of cycloarenes is that they can serve as models for defects in graphene thanks to its cavity structure,[2,9] and help us better understand and make use of some unique properties of defected graphene.[10,11]

In addition, due to their peculiar electronic structures, cycloarenes can also serve as ideal platforms to investigate fundamental questions related to the concept of aromaticity.[12–14] Kekulene is probably the most representative example in this respect.[15] The synthesis and characterization of kekulene,[1,16,17] answered a long-standing controversial question about arenes and their nature of aromaticity: do π electrons delocalized throughout the whole conjugated system, as hypothesized by Pauling,[18] or do they remain localized on sextets, as predicted by McWheeny[19] and described phenomenologically by Clar?[20] X-ray crystallographic analysis and NMR measurements in high-boiling-point solvents revealed a local aromatic character that π-electrons are localized on individual benzene-type rings for the kekulene, which was further confirmed by ultra-high-resolution atomic force microscopy (AFM)[15] and modern on-surface synthesis.[21] Although some new synthetic methods have been explored over the years,[4,8,22] only a few cycloarenes were reported,[5] such as edge-extended kekulenes,[23,24] septulene,[22] and octulene,[4,8] due to the challenging synthesis of this kind of cata-condensed aromatic macrocyclic systems,.[5,15] The lack of molecular diversity greatly limits the further development of cycloarenes and related analogs.

The molecular shape of kekulene is like an equiangular superhexagon with each side

characterized as the structure of acene with zigzag edges.[25] We can use six parameters to represent the lengths of hexagon sides and uniquely specify the hexagon. In fact, in 2021, Wu and co-workers[23] used the notation, $[m, n]$, proposed by Bergan et al.,[26] to describe the structure of the core-expanded kekulenes, named $[m, n]$cycloarenes, where m and n represent the number of benzene rings on each of the three longer and each of the three shorter zigzag-like edges, respectively. However, such a nomenclature applies only to structures with alternating side lengths, thus covering only a specific type of the extended kekulenes. In addition, other edge-extended homologues of kekulene were designed and synthesized by Lu and co-workers[24] through the similar method in 2023. In light of successfully synthesized extended kekulenes, we hope to further extend kekulene to a more generalized structure, such that the lengths of the six sides can be any positive integers, and therefore fully enrich the structural diversity of this type of molecules.

In fact, in our previous work,[27] we proposed the generalized kekulenes, removing the structural constraints in the definition of the expanded kekulenes[23] so that the hexagon-shaped macrocycles can a variable length for all six sides. We also conceived a new type of cycloarenes, named, clarenes.[27] While generalized kekulenes have zigzag-like edges, clarenes have armchair-like edges and thus always achieve the maximum possible number of Clar sextets.[20,28,29] Hence, clarenes are shown to be generally more electronically stable than generalized kekulenes.[27] We made use of generalized kekulenes and clarenes as molecular building blocks to construct generalized infinitenes.[27] Nonetheless, we have not previously provided the details about the design of generalized kekulenes and clarenes, neither have we presented a comprehensive study on the structures, stability, and properties for these novel cycloarenes.

In this work, we have systematically investigated generalized kekulenes and clarenes, and determine the lowest-energy isomers of various sizes through systematic quantum chemical calculations, thereby elucidating the factors that determine their stability. For very large clarenes, we also conduct a conformational study due to the flexibility of their molecular

structures. Finally, in order to identify these new compounds in future synthesis, we have further simulated ^{1}H NMR and UV-vis spectra for the most stable isomers with different sizes.

2 Computational Details

We enumerated all initial structures of generalized kekulenes and clarenes using our open-source code GenInfi.[30] We performed geometry optimizations and vibrational frequency analyses, which verify the energy minima on the potential energy surface using the GFN2-xTB method[31,32] implemented in the XTB program (version 6.3.3).[31,33,34] We refined the xTB results at the DFT level for the lower-energy isomers according to the xTB relative energies (see Section 1 in ESI for details).

All DFT and time-dependent (TD) DFT computations were performed with the GAUSSIAN 16 package.[35] We carried out geometry optimizations at the B3LYP/6-31G* level of theory[36,37] in conjunction with the D3(BJ) dispersion correction.[38] The nature of the stationary points was confirmed by subsequent frequency calculation. Our assessment calculations showed that the relative isomer energies obtained from the GFN2-xTB calculations are consistent with those obained at the B3LYP-D3(BJ)/6-31G* level (see Fig. S1 in ESI). For the lowest-energy isomers, we proceeded to optimize the geometries using the ωB97XD[39] functional, coupled with the larger cc-pVDZ basis set,[40] which is designed to handle self-interaction errors in DFT more effectively,[41] thereby providing a more accurate description of π-delocalized systems.[42] As shown in Fig. S2 in ESI, the ωB97XD/cc-pVDZ predicted geometries are in a general agreement with the experimental values measured by X-ray diffraction (XRD). Additionally, Fig. 5 and Fig. S3 in ESI show that the relative energies calculated at the B3LYP-D3(BJ)/6-31G* level are consistent with the ωB97XD/cc-pVDZ results for all considered looped polyarenes of a varying size. We have applied Grimme's quasi-rigid-rotor harmonic oscillator treatment[43] for vibrational modes with frequencies lower than 100 cm^{-1}

in order to reasonably evaluate Gibbs free energies, as implemented in the SHERMO program (version 2.3.5).[44]

The combinatorial enumerations[29,45] of Clar structures[20,28,29] were conducted by our open-source program EZRESON[46–48] (version 3.0). To visually reveal the π-π stacking interactions, we computed isosurfaces of interaction region indicator (IRI)[49] mapped with sign(λ_2)ρ function[49] by using the MULTIWFN version 3.8.[50] The isosurface maps were rendered by the VMD program (version 1.9.3).[51]

The nuclear magnetic resonance (NMR) computations were carried out at the B3LYP/6-311+G(2d,p) level in conjunction with gauge-including atomic orbitals (GIAOs) on the basis of the ωB97XD/cc-pVDZ optimized geometries. We choose l,2,4,5-tetrachlorobenze ($PHCl_4$) as a solvent with the solvation model based on the density (SMD) to simulate the experimental environment.[52] Based on our previous simulations of ^{1}H NMR spectra for the experimentally synthesized [12] and [20]K-infinitenes, which agree well with the experimental spectra,[27,53–55] we also applied in this work the empirical scaling technique with appropriate scaling factors using calibrated parameters to achieve a balance between precision and computational efficiency.[56–59] With the support of the Multiwfn program, we gained ^{1}H NMR spectra for the considered compounds in l,2,4,5-tetrachlorobenze solvent. As shown in Fig. S5 in ESI, our simulated ^{1}H NMR spectrum for [12]kekulene is in good agreement with the experimental one.

We performed TD DFT calculations at the B3P86/6-311G(d,p) level[60,61] to simulate the UV-vis absorption for the lowest-energy kekulenes and clarenes from 8 to 60 rings, based on the ωB97XD/cc-pVDZ optimized geometries. Our previous work on simulation of UV-vis absorption spectra for experimentally synthesized [12] and [20]K-infinitenes has shown the consistent results between simulated and experimental spectra.[27,53–55] Excitation calculations were performed for a total of 100 states. With the same DFT functional, we also tried a larger basis set, 6-311++G(2d,p), but the results did not improve significantly, indicating that the 6-311G(d,p) is sufficient to describe the considered compounds (see Fig. S13 in ESI).

Our simulated UV-vis absorption spectra for the experimentally synthesized [12]kekulene is in reasonable agreement with the experimental ones (see Fig. S14 in ESI).[23,62]

3 Results and Discussion

3.1 Generalized kekulene and clarene structures

Edge-extended kekulene derivatives with 14 and 16 rings have been synthesized by Lu and co-workers,[24] which were constructed by extending a pair of opposite sides of the kekulene molecule. In addition, Wu also synthesized the similar molecules with alternating side lengths.[23] We may further generalize the kekulene structure by allowing all six sides of the superhexagon shape to have a variable length. In our previous work,[27] we mentioned such a generalization of kekulene structures, and here we provide more specific details in this aspect. We define the generalized kekulenes (hereinafter simply referred to as *kekulenes* for brevity), as a new type of single-layered cycloarene, to have a planar equiangular hexagonal structure, and the six sides are all linearly fused benzene rings, that is, following a zigzag type of arrangement.[25] Fig. 1(a) illustrates the concept of kekulenes, exemplified by one of the experimentally synthesized kekulene, [2,2,4,2,2,4].[24] The numbers in brackets indicate the side lengths, meaning the effective number of benzene rings along each side of the superhexagon for the given kekulene structure. Note that each of these numbers is one fewer than the actual number of benzene rings.[27] The sum of all six side lengths equals the total number of rings in the entire molecule.

For kekulenes with a fixed number of rings, we can construct many possible isomers with different equiangular hexagonal structures based on the above concept. More detailed construction procedures are described in Section 6 in ESI. Valid side lengths of the superhexagon, h_1, h_2, h_3, h_4, h_5, and h_6, are positive integers greater than or equal to 1, and the sum of them is equal to the total number of rings in kekulene, N_{ring}. We can construct the corresponding kekulene, [h_1, h_2, h_3, h_4, h_5, h_6], based on the above rules, where square

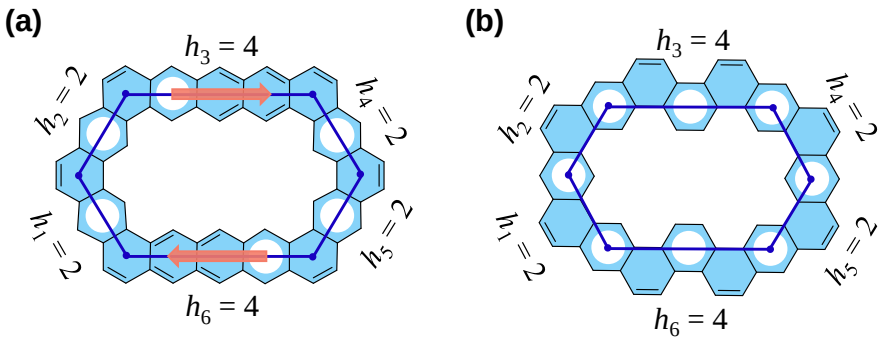

[16]Kekulene: [2,2,4,2,2,4]

(Experimentally synthesized)

$N_{\text{sextet}} = 6$

RE = 20.5 kcal/mol

[16]Clarene: <2,2,4,2,2,4>

(Theoretically proposed)

$N_{\text{sextet}} = 8$

RE = 0.0

Figure 1. Structural definition of (a) the experimentally synthesized generalized kekulene [2,2,4,2,2,4][24]and (b) the isomeric clarene <2,2,4,2,2,4>, the lowest-energy form of [16]cycloarenes. The superhexagon formed by benzene rings are indicated by blue lines. The structural notation of a kekulene or a clarene is determined by the side lengths of superhexagon (h_1, h_2, h_3, h_4, h_5, and h_6). The white circles represent Clar sextets. The brick red arrows in (a) show the migration of sextets. The numbers of sextets (N_{sextet}) for both molecules and the relative energies (RE) between them calculated at the ωB97XD/cc-pVDZ level are provided in kcal/mol.

brackets are used to represent a kekulene. Given a specific kekulene, the name may not be unique, and different names like [h_2, h_3, h_4, h_5, h_6, h_1] and [h_1, h_6, h_5, h_4, h_3, h_2] may correspond to identical kekulene structure. We can select any starting edge and loop six edges in a fixed direction whether clockwise or counter-clockwise, which is circular equivalent. For kekulene [2,2,4,2,2,4] in Fig. 1(a), we also call it [2,4,2,2,4,2] or [4,2,2,4,2,2], both of them being equivalent. Note that coronene can be regarded as the simplest kekulene, [1,1,1,1,1,1]. While the expanded kekulenes proposed and synthesized by Wu and co-workers,[23] denoted by $[m, n]$, which are only limited to structures with alternating side lengths, the structures and nomenclature we have proposed are more general. Note that kekulenes of other polygonal shapes, such as quintulene shaped as pentagon,[63] septulene shaped as heptagon,[22] and octulene shaped as octagon,[4,8] exhibit nonplanar geometries and are significantly less stable due to considerable strain. Hence, it is logical to consider solely on hexagon-shaped kekulenes, as they are anticipated to possess a planar and consequently strain-free structure.

Although the planar structure promotes the stability of kekulene, π stabilization becomes less favorable as the ring size increases. According to the Clar rule,[20,28,29] kekulenes with side lengths greater than 2 fail to achieve optimal π stabilization because they do not achieve the maximum number of Clar sextets and the sextets are thus migrating[64](see Fig. 1(a) as an example). In addition, it is known that acenes with 6 or more rings have an open-shell polyradical character in electronic structure, such as hexacene.[65] Consequently, kekulenes with sufficiently long sides are probably not stable, similar to the case of acenes. In view of this, we come up with a new kind of planar single-layered cycloarene with armchair-type edges, which are termed as clarene[27] because they always possess the maximum possible number of Clar sextets ($N_{\mathrm{ring}}/2$). Note that clarenes can have only even-numbered side lengths due to the armchair fashion, while the side lengths of kekulenes can be any positive integer. Fig. 1(b) shows the molecular structure of [16]clarene <2,2,4,2,2,4>, an isomer of [16]kekulene shown in Fig. 1(a), where angle brackets are represented to a clarene. Like kekulenes, the nomenclature of clarenes is also circularly equivalent, that is to say, <2,2,4,2,2,4>,

<2,4,2,2,4,2>, and <4,2,2,4,2,2> represent the same structure. Clarenes also have a similar molecular structure to kekulenes with a superhexagon shape, with the difference that the benzene rings on each side have an armchair-type arrangement.[25] Moreover, the original (not generalized) kekulene molecule, equilateral [12]kekulene [2,2,2,2,2,2], is also regarded as [12]clarene <2,2,2,2,2,2>.[1,15–17]

In terms of electronic structure, [16]clarene has generally more favorable stabilization than [16]kekulene, as evidenced by the numbers of Clar sextets (8 vs 6 as shown in Fig. 1), and Hückel molecular orbital (HMO) π energies ($-91.6|\beta|$ vs $-91.1|\beta|$). DFT calculation also shows that [16]clarene is energetically more stable than experimentally synthesized [16]kekulene with an appreciable energy difference, 20.5 kcal/mol.

In this work, we investigate systematically the kekulenes and clarenes with a wide range of rings from 8 to 60 rings. We have enumerated a complete set of these structures based on the aforementioned construction procedure. Table 1 summarizes the numbers of all considered isomers of kekulenes and clarenes for each of the considered numbers of rings, N_{ring}.

3.2 Relative stability of kekulene and clarene isomers

3.2.1 Relative stability of kekulene isomers

We first discuss kekulenes containing 8 to 60 rings. We have tested all considered kekulene isomers with up to 32 rings using DFT calculation, and find the relationship between N_{ring} and spin multiplicity of ground state for these kekulene isomers. We find that the ground state has a closed shell configuration for all kekulene isomers with $N_{\text{ring}} \leq 15$. For kekulenes of $N_{\text{ring}} \geq 16$, the ground state of many isomers is an open-shell singlet. In addition, there is also a certain relationship between side length of the superhexagon and the spin multiplicity of ground state for these kekulene isomers. For kekulenes with side lengths greater than or equal to 7, ground state is an open-shell singlet, while ground state has a closed shell for kekulenes with a maximum side length less than or equal to 5, except [18]kekulene, [1,5,1,5,1,5], which is 2.4 kcal/mol lower than its closed-shell state at ωB97XD/cc-pVDZ

Table 1. Number of isomers for different types of equiangular hexagonal kekulenes and clarenes with a varying number of rings.

N_{ring}	Kekulene	Clarene	N_{ring}	Kekulene	Clarene
8	1	—	28	33	5
9	1	—	30	42	4
10	2	—	32	48	7
11	1	—	34	57	5
12	4	1	36	69	11
13	2	—	38	69	7
14	5	—	40	90	13
15	4	—	42	106	11
16	7	1	44	118	17
17	5	—	46	134	13
18	11	1	48	154	23
19	7	—	50	170	17
20	13	2	52	190	27
21	11	—	54	215	23
22	17	1	56	235	33
24	23	4	58	260	27
26	27	2	60	290	42

level. The boundaries between the closed-shell and open-shell singlet states are blurry for kekulenes with a maximum side length equal to 6. For kekulenes of $N_{\text{ring}} > 32$, the ground state of almost all isomers is an open-shell singlet, and we therefore only determine the lowest-energy structures with a varying number of rings by quantum chemical calculations. After determining the ground state of these isomers based on DFT calculations, we compare the relative energies between kekulene isomers and look for the factors that govern the relative stability.

According to the definition of kekulenes in Section 3.1, we know that kekulenes do not achieve the maximum number of Clar sextets, and therefore, π delocalization should be important for the stability of kekulene isomers. So, we have tried to use the simple HMO theory[66–69] to interpret the stability of the isomers. In fact, we have successfully predicted the relative stability of generalized infinitenes[27] and CNBs[70] based on the HMO theory. Fig. 2(a) plots the relative energies of all 11 isomers of [18]kekulenes against their HMO π energies. As we can see, the data points show a linear correlation with high squared correlation coefficient ($R^2 = 0.984$) between the relative isomer energy and the HMO energy, confirming that π stabilization is indeed the decisive factors in isomer stabilities. Note that two isomers of [18]kekulenes have been successfully synthesized experimentally, namely, [3,3,3,3,3,3] (see Fig. 2(b)) and [2,4,2,4,2,4] (see Fig. 2(c)). As shown in Fig. 2(a), both of the experimentally synthesized isomers (black filled circle) exhibit relatively high stability with a π energy lower than other [18]kekulenes, though they all do not achieve the maximum number of Clar sextets.

Althougth the HMO theory is not able to reasonably describe open-shell structures, the HMO π energies still correlate well with the DFT relative energies including the open-shell singlet cases (see black hollow triangle in Fig. 2(a)). The above conclusion is generally valid for the kekulenes of other sizes (see Fig. S28–S29 in ESI). For kekulene isomers with an open-shell singlet electronic structure, as shown in black hollow triangle in Fig. 2(a), we can understand it from the competition between the fulfillment of maximum number of

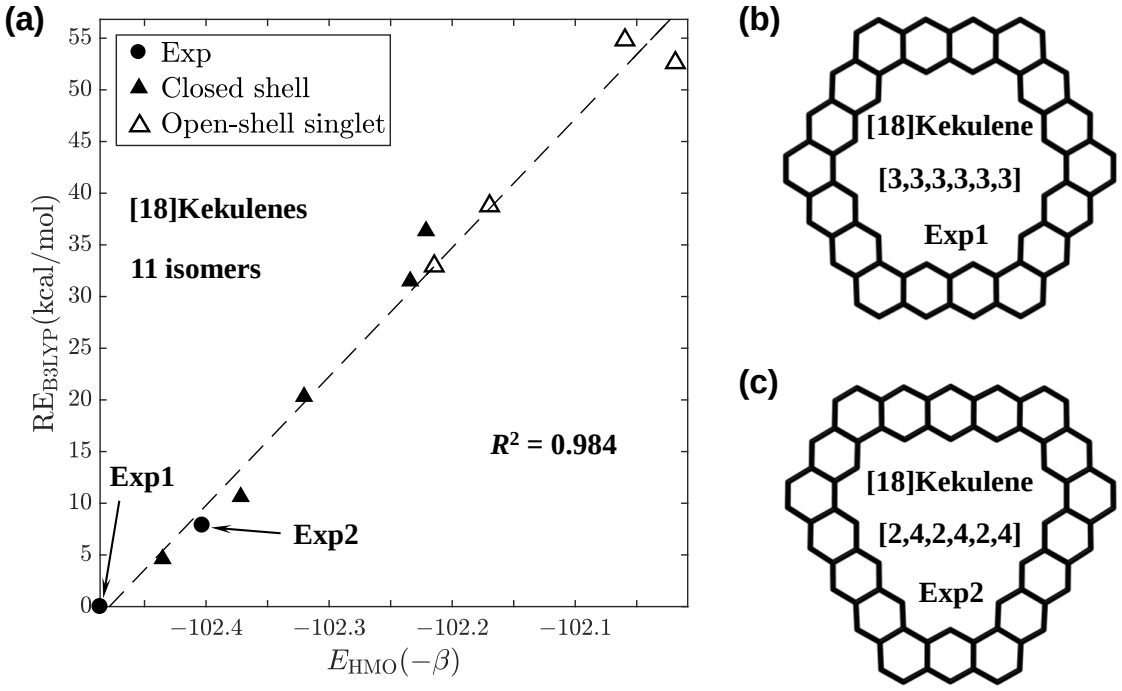

Figure 2. (a) DFT relative energies, $\mathrm{RE_{B3LYP}}$, versus HMO π energies, E_{HMO}, for [18]kekulenes. Experimentally synthesized structures are indicated by black filled circle. Closed shell structures and open-shell singlet structures are represented by black filled triangle and black hollow triangle, respectively. Squared correlation coefficient (R^2) is provided. ωB97XD/cc-pVDZ optimized structure of experimentally synthesized [18]kekulenes (b) [3,3,3,3,3,3] and (c) [2,4,2,4,2,4]. Hydrogen atoms are omitted for clarity. The isomers marked Exp1 and Exp2 in (a) correspond to the structures in (b) and (c), respectively.

Clar sextets, and the avoidance of having polyradical configuration. Let us take acene as an example,[65] according to Clar's aromatic π-sextet rule,[20,28,29] the maximum possible number of Clar sextets for an acene is only 1 so as to ensure a closed-shell electronic structure. For shorter acenes with the number of linearly fused benzene rings less than 6, the π energy is not optimal because of the limited number of Clar sextets. As the size of acene increases, the number of Clar sextets increases in order to gain a higher stability, at a cost of forming radical resonance structures, which would destablize the system.[65] The same goes for kekulenes since each edge of kekulene can be regarded as a acene structure. For relatively large kekulenes with more than 32 rings, due to the open-shell electronic structure, we only investigate a few representative systems (see Table S1 in ESI).

3.2.2 Relative stability of clarene isomers

In parallel to keulenes, we have computed clarene isomers with 12 to 60 rings by DFT. We find that clarenes with $N_{\text{ring}} < 40$ have a perfectly planar structure, while some molecular structures of larger clarenes are distorted from planarity due to $\pi-\pi$ stacking. Therefore, we will discuss below the relative stability of these two different sizes of clarene structures separately.

Let us first discuss the case of smaller clarene isomers with $N_{\text{ring}} < 40$, in order to find out the key factors governing their relative stability. Unlike kekulenes, clarenes have the maximum possible number of Clar sextets, implying that all of the clarene isomers should have similar π stabilization. Nevertheless, we have also applied the simple HMO theory to evaluate the π energies of clarene isomers. As shown in Fig. 3, π energy predicted by HMO still have a good correlation with the relative energies of [28] and [30]clarene isomers calculated by DFT. These results show that the relative stability of smaller clarene isomers is also determined by π energy. The impact of strain on stability can be practically ignored because smaller clarenes all have planar structures. The same conclusion is reached for clarenes of other sizes with $N_{\text{ring}} < 40$ (see Fig. S23 in ESI). Moreover, we can understand

the relative isomer stability more intuitively by using the Clar rule.[20,28,29] All clarene isomers have one and only one Clar structure with the same number of Clar sextets ($N_{\text{ring}}/2$). Thus, the Clar rule cannot distinguish the difference in π stabilization between clarene isomers. Nevertheless, the number of Clar resonators[29] (see Fig. S35 for explaination in ESI) with the second largest number of sextets is different for these isomers. As shown in Fig. 3(a) and (b), a clarene isomer with a larger number of secondary Clar resonators (represented by bold numbers) is energetically more stable. For the first two isomers with the lowest energy of [30]clarenes, as shown in Fig. 3(b), they have the same number (33) of secondary Clar resonators, and we then compare the number of the Clar resonators with the third largest number of sextets to explain the π stabilization between them. As the lowest-energy isomer has more tertiary Clar resonators than the second lowest-energy isomer (372 vs 348, see numbers in brackets), it is understandable that the former is more stable than the latter.

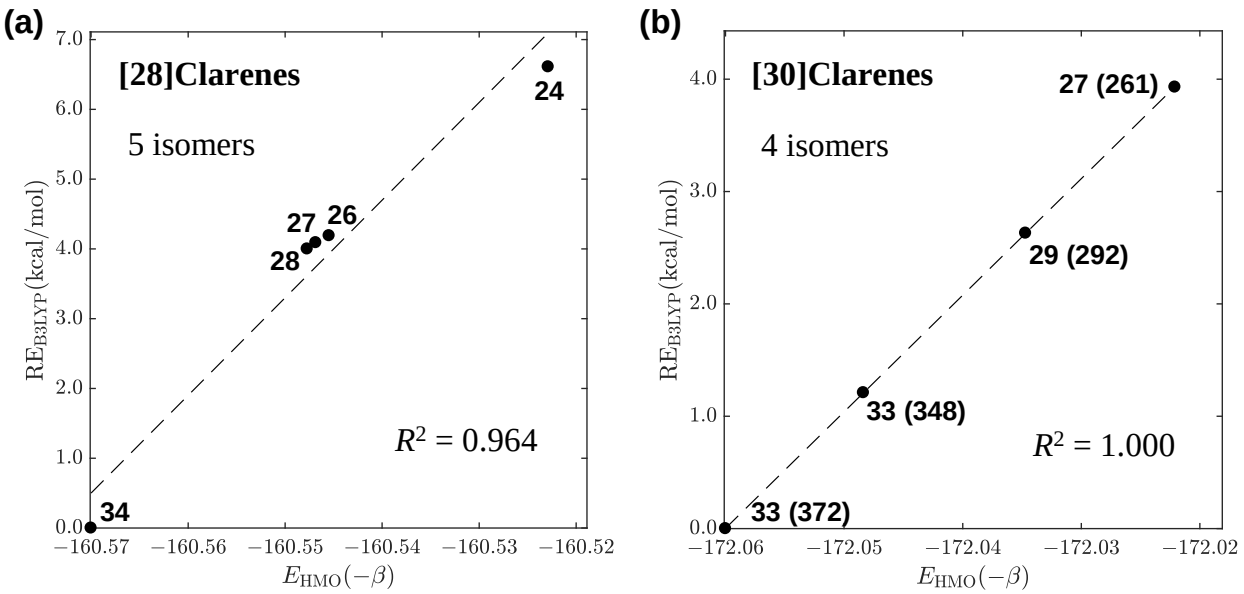

Figure 3. DFT relative energies, RE_{B3LYP}, versus HMO π energies, E_{HMO}, for (a) [28]clarenes, (b) [30]clarenes. The number of secondary Clar resonators are represented by black bold numbers. Numbers in brackets indicate the Clar resonators with the third largest number of sextets. Squared correlation coefficients (R^2) are provided.

We also find the molecular structures of clarenes with the number of rings that are multiples of 4 are distorted due to $\pi-\pi$ stacking as $N_{\text{ring}} \geq 40$ and more stable than other

clarene isomers (see Fig. 4(a) and Fig. S24 in ESI). Clarenes that meet the above conditions all have the similar structures characterized by stadium-type structure and are named as $<2,2,2k,2,2,2k>$, (the integer $k \geq 8$) (see Fig. S27(a) in ESI). Because of the larger molecular size and specific geometric characteristics, the two extremely long opposite sides of the superhexagon exhibit enough flexibility to approach each other to effectively induce intramolecular $\pi-\pi$ stacking interaction, which in turn leads to the distortion of the molecular structure.

For larger clarenes with $N_{\text{ring}} \geq 40$, we find that the relative isomer energy spans a much wider range than in the case of the smaller clarenes with $N_{\text{ring}} < 40$. As shown in Fig. 4(a) and (b), in general, HMO π energies has a good correlation ($R^2 = 0.999$) with the DFT relative isomer energies for all isomers but the lowest-energy one, which suggests that π delocalization generally determines the relative stability for most of the clarene isomers. Note that the outlier (hollow circle) obviously deviates from the correlation line and this exceptional point corresponds the lowest-energy isomer. Fig. 4(c) shows the ωB97XD/cc-pVDZ optimized molecular structure for the lowest-energy isomer of [48]clarene, <2,2,20,2,2,20>. It is obvious that the stadium-type structure is significantly distorted as a result of the strong $\pi-\pi$ stacking interactions between the two longest opposite sides (see IRI map[49] in Fig. 4(a) and Fig. S25–S26 in ESI), as mentioned in Section 3.2.2. Although the distortion will inevitably cause an increase in strain, the stabilization effect brought by $\pi-\pi$ stacking still dominates. As a result, as shown in Fig. 4(a), this $\pi-\pi$ stacking clarene isomer gains quite a lot additional stability, which can be clearly seen from the intercept of the y axis with 20.8 kcal/mol. The same conclusion generally holds for the clarenes of other sizes (Fig. S24 in ESI).

However, for the equiangular stadium-type structures (see the schematic structure of [48]clarene isomer, <2,2,20,2,2,20>, in Fig. 4(c) as an example), $\pi-\pi$ stacking is only possible when the number of rings is a multiple of 4, as mentioned in Section 3.2.2. For [54]clarenes, all equiangular structures have relatively much higher energy (see Fig. 4(b))

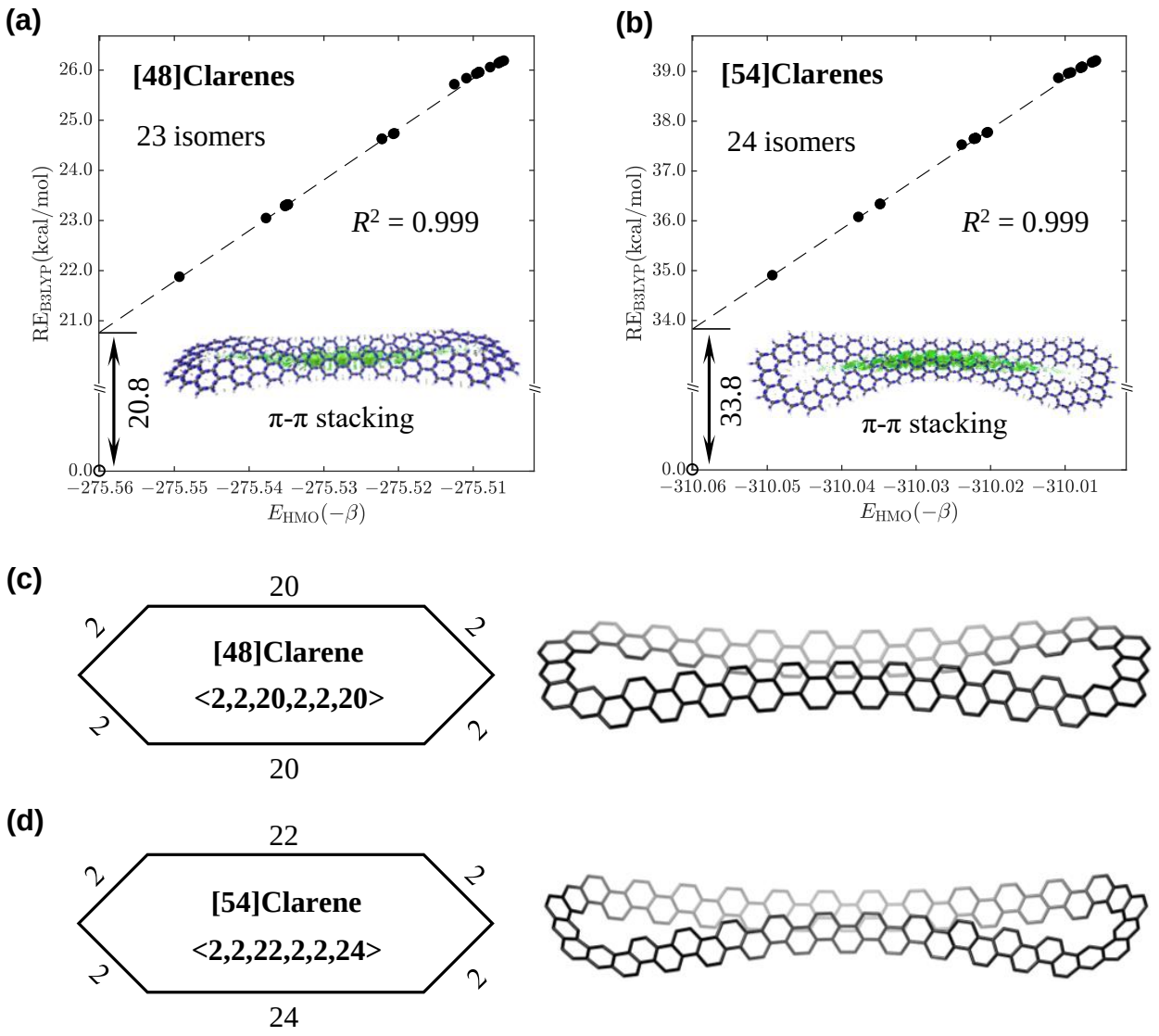

Figure 4. DFT relative energies, RE_{B3LYP}, versus HMO π energies, E_{HMO}, for (a) [48]clarenes and (b) [54]clarenes. Structures with $\pi-\pi$ stacking are indicated by hollow symbols, and IRI maps for $\pi-\pi$ stacking are also provided in each plot. The intercept of the y-axis in (a) and (b) represents $\pi-\pi$ stacking effect. Squared correlation coefficients (R^2) in (a) and (b) are only for data points with filled symbols. Structure diagram and the ωB97XD/cc-pVDZ optimized structures of the lowest-energy isomer of (c) [48]clarene, <2,2,20,2,2,20> and (d) [54]clarene, <2,2,22,2,2,24>. The numbers in (c) and (d) represent the side lengths of the stadium-type clarene. Hydrogen atoms are omitted for clarity.

and no $\pi-\pi$ stacking is present since there are no stadium-type structures for equiangular hexagonal clarenes whose number of rings is not a multiple of 4. Considering the additional high stabilization effect brought by $\pi-\pi$ stacking, for clarenes with the number of rings that is not a multiple of 4, we have additionally investigated nonequiangular hexagonal clarenes with similar stadium-type structures to obtain more stable isomers of the same molecular size (see the schematic structure of [54]clarene isomer, <2,2,22,2,2,24>, in Fig. 4(d) and Fig. S27(a) for explanation of construction method in ESI). Similar to [48]clarene, <2,2,20,2,2,20>, the structure of [54]clarene, <2,2,22,2,2,24>, also has obvious distortion caused by $\pi-\pi$ stacking. The IRI map[49] for <2,2,22,2,2,24> also confirms the existence of the significant $\pi-\pi$ stacking with stabilization effect being 33.8 kcal/mol in energy, as shown in (Fig. 4(b) and S36–S37 in ESI). The same conclusion also generally holds for the clarenes of other sizes (Fig. S24 in ESI).

3.2.3 $\pi-\pi$ stacking conformers

For the large-sized infinitenes studied in our previous work,[27] the $\pi-\pi$ stacking plays an important role in their structures and stability, but we have not further studied whether this effect would lead to different conformers. The structures of stadium-type clarene isomers are distorted due to $\pi-\pi$ stacking, as mentioned in Section 3.2.2. So, we need to consider different conformers of them and the stability of these conformers since they have greater flexibility. Therefore, we have investigated different conformers of the stadium-type structure of [60]clarene, <2,2,26,2,2,26>, since they have obvious $\pi-\pi$ stacking. In addition, we have also considered the nonequiangular stadium-type structures of [60]clarene, <2,2,24,2,2,28> and <2,2,22,2,2,30> (see Fig. S27(b) in ESI for structural details), because they also have obvious $\pi-\pi$ stacking.

We have searched all possible conformers for each isomer, 37 in total (see Table S3 in ESI). We find that the relative shift of the longest opposite sides of [60]clarenes makes it possible for clarenes to have some different conformers (see Fig. S38 in ESI). For [60]clarene

<2,2,22,2,2,30>, we find two distinct conformers with a small energy difference of 2.7 kcal/mol. The structural difference between the two conformers lies in the relative positions of the longest opposite sides of clarene (see Fig. S38(c) and (d) in ESI). Compared with more symmetric conformer, the more asymmetric conformer is more stable. Note that all conformers of <2,2,22,2,2,30> are actually not stable, being at least 38.6 kcal/mol higher in energy than the lowest-energy isomer, <2,2,26,2,2,26>. However, for [60]clarene, <2,2,24,2,2,28>, all conformers are similar to each other with almost same energy, and are actually also less stable than <2,2,26,2,2,26>, being 9.2 kcal/mol in energy. The conformers of [60]clarene, <2,2,26,2,2,26>, are also similar to each other with energy difference within 1.0 kcal/mol.

3.2.4 Relative stability of kekulenes, clarenes, and other looped polyarenes

Now we discuss the lowest-energy isomer among all kekulenes and clarenes of all considered sizes (see Fig. S30–S34 for the detailed molecular structures and Tables S1 and S2 for their relative energies in ESI). In fact, our thorough and systematic calculations, encompassing the enumeration of all possible isomeric shapes of the superhexagon, indicate that clarenes are generally significantly more energetically stable than kekulenes of the same size. Fig. 5 presents the relative energies of the lowest-energy kekulene and clarene isomers, and many other typical cyclopolyarenes used to represent looped polyarenes,[27] including the experimentally synthesized isomers with respect to armchair CNBs, in variation with N_{ring}. Additionally, we have compared the Gibbs free energies (at 298.15 K and 1 atm) of these cyclopolyarenes, and they exhibit the same trend as observed in terms of electronic energies (see Fig. S3–S4 in the ESI).

Armchair CNBs as a typical form of CNBs have the most favorable π stabilization with the maximum number of Clar sextets and relatively less severe strain, which exhibits an inverse proportionality to molecular size. For this reason, numerous armchair CNBs with both regular[71–73](filled green up triangles) and irregular edges[72,74–78] (filled Persian green right triangles) have been successfully synthesized in the laboratory, encompassing a range

of 10[71–73] to 42[77] rings. In addition, as we can see in Fig. 5, zigzag CNBs (blue down triangles) are all open-shell singlets, and thus have a high relative energy (e.g., 41.0 kcal/mol for $N_{\text{ring}} = 8$), which grows almost linearly with the increasing number of rings. It is worth noting that the group of Wang has observed [8]zigzag CNB derivative by high resolution mass spectrometry (HRMS).[79] Infinitenes are also the novel molecules and are attracting an increasing attention very recently. Indeed, so far, only three infinitenes (black diamonds) have been synthesized by Itami[53] and Wu[54,55,80] in the laboratory with 12, 16 and 20 rings, as shown in Fig. 5. In addition, not long ago, we have proposed the concept of infinitene family and have elucidated the stability rules for them.[27]

As shown in Figure 5, for small sizes with $8 \leq N_{\text{ring}} \leq 15$, kekulenes are the energetically most stable structures among all cyclopolyarenes under consideration due to less strain compared to armchair CNBs. As the molecular size increases, overall, the stability of kekulenes gradually decreases compared to armchair CNBs. The maximum number of Clar sextets for kekulene isomers are only six, which make π delocalization stabilization of kekulenes gradually abate as the size of molecules increases. As a result, the relative energy of kekulenes, in comparison to armchair CNBs, becomes less negative, indicating that they are energetically less stable than armchair CNBs for $N_{\text{ring}} \geq 24$. Note that some lowest-energy kekulenes predicted by this work have been successfully synthesized in the laboratory with number of rings from 10 to 21.[1,15–17,23,24,81] In addition, some kekulenes with retalively high energy have also been synthesized, such as, [14], [16], and [18]kekulenes.[8,22–24]

Finally, as we can see, clarenes with $16 \leq N_{\text{ring}} \leq 60$ are the energetically most stable. Compared to kekulenes that have the limited number (six) of Clar sextets when they are large enough, clarenes always have a maximum number ($N_{\text{ring}}/2$) of Clar sextets, which make them possess a maximized π stabilization and generally more stable than kekulenes. On the other hand, the energy of clarenes with $N_{\text{ring}} < 40$ relative to armchair CNBs is getting less negative, because the strain of armchair CNBs is released as the size increases. However, the relative energy of clarenes with $N_{\text{ring}} \geq 40$ shows two diverging trends as the molecular size

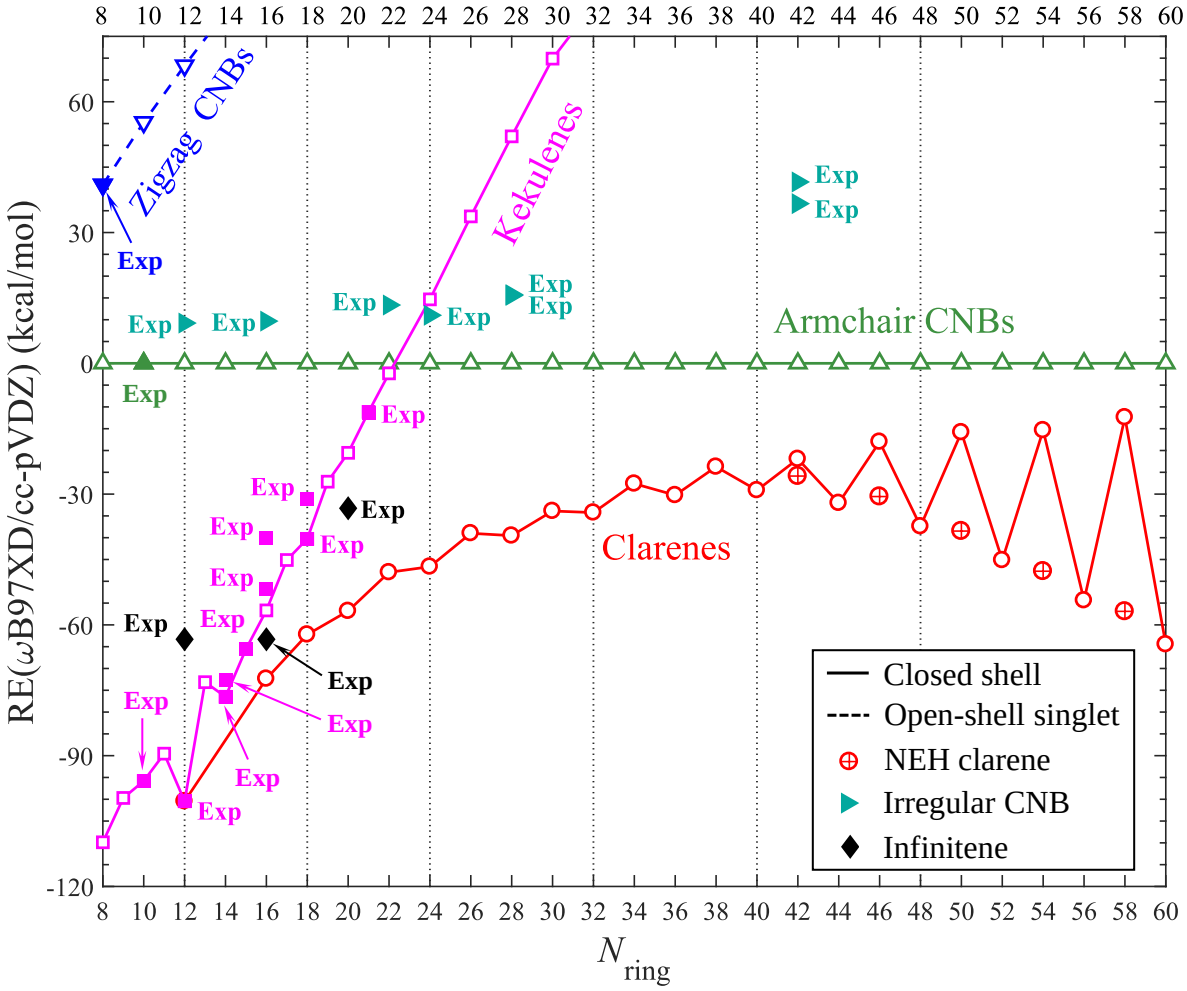

Figure 5. Relative energy of different typical forms of cyclopolyarenes with different number of rings, as calculated at the ωB97XD/cc-pVDZ level. Experimentally synthesized structures[1,15–17,23,24,53–55,71–78,80,81] are indicated by filled symbols. The circled plus symbol represent the nonequiangular hexagonal clarenes (NEH clarenes).

increases. Stadium-type clarenes with N_{ring} being a multiple of 4 become gradually more stable than the armchair CNBs due to intramolecular $\pi-\pi$ stacking interactions (see Fig. S24–S26 in ESI). Remarkably, as we can see in Fig. 5, very large clarenes display noticeably high thermodynamic stability. For instance, [60]clarene is 64.5 kcal/mol lower in energy than [60]armchair CNB. On the other hand, clarenes with N_{ring} that is not a multiple of 4 follow the similar tendency to that for the clarenes of $N_{\text{ring}} < 40$, due to the lack of $\pi-\pi$ stacking.

As mentioned in Section 3.2.2, we have additionally considered the nonequiangular stadium-type isomers of clarenes to introduce $\pi-\pi$ stacking (see Fig. S27 in ESI). As shown in Fig. 5 (indicated by circled plus symbol), nonequiangular stadium-type isomers have a tendency to become more stable than equiangular isomers, as the molecular size increases and have a notably lower energy compared to equiangular isomers with the same N_{ring} (from 3.9 to 44.5 kcal/mol), thanks to extra stabilization effect from $\pi-\pi$ stacking (see Fig. S36–S37 in ESI). Note that although all clarene isomers except [12]clarene, which can also be regarded as [12]kekulene, have not been synthesized in the laboratory, their remarkable thermodynamic stability suggests the viability of the synthesis of these clarenes.

3.3 Spectroscopic properties of the lowest-energy isomers of kekulenes and clarenes

We have performed ^{1}H NMR and UV-vis simulations for the lowest-energy kekulene and clarene structures, in order to facilitate the experimental characterization of the predicted structures.

3.3.1 ^{1}H NMR spectra for the lowest-energy isomers of kekulenes and clarenes

Fig. 6 presents the simulated ^{1}H NMR spectra for the lowest-energy isomers of [9]kekulene, [20]kekulene, [24]clarene, and [38]clarene (see Fig. S6–S12 in ESI for the ^{1}H NMR spectra of the kekulenes and clarenes of other sizes). Obviously, there are three groups of peaks corresponding to three types of H atoms in both kekulene and clarene structures.

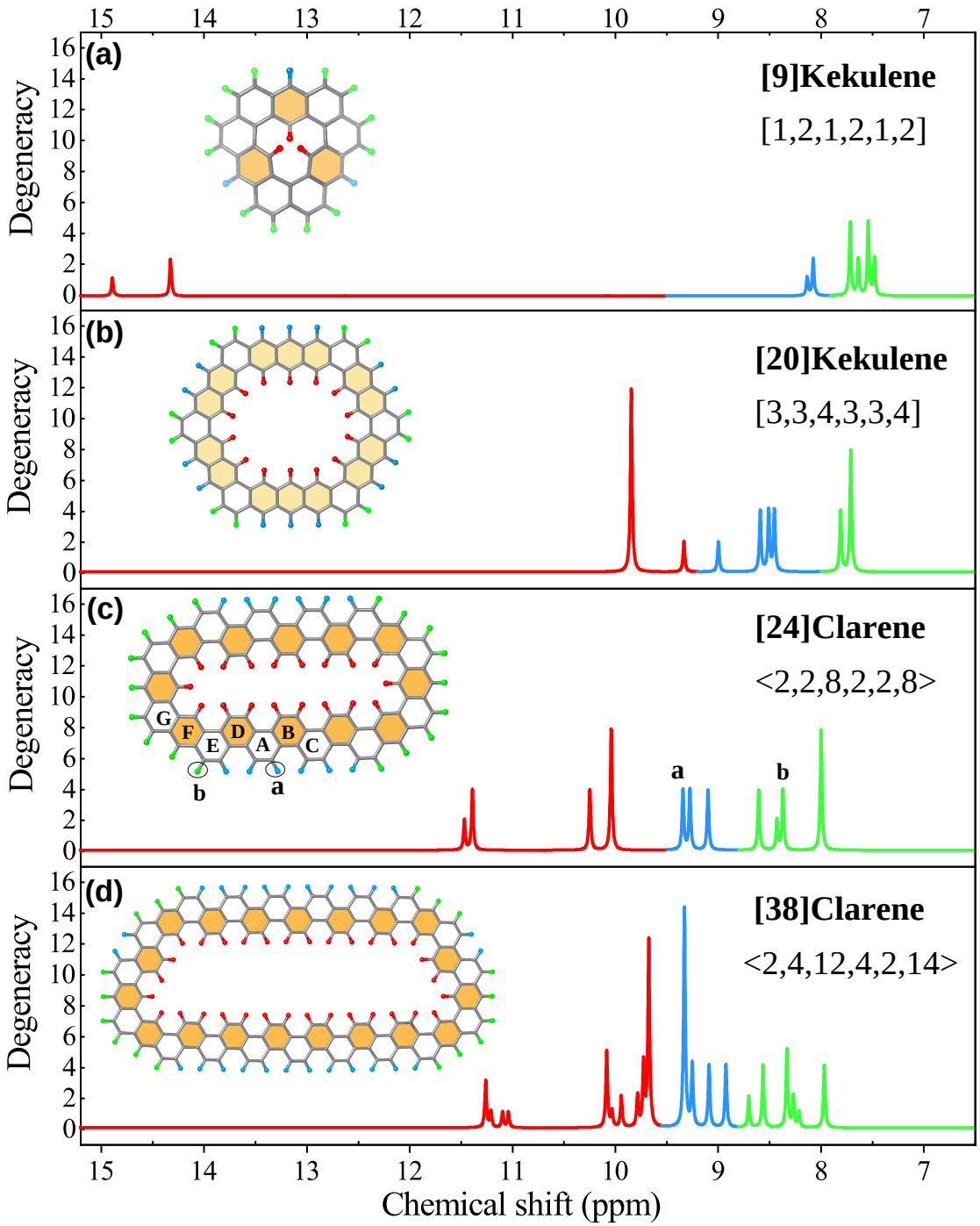

Figure 6. Simulated ^{1}H NMR spectra of the lowest-energy isomers of (a) [9] and (b) [20]kekulenes, (c) [24] and (d) [38]clarenes in $PHCl_4$ solution. The peaks are classified into three groups, distinguished by red, blue, and green colors originated from the corresponding H atoms in the illustrated structure, which are indicated in the same color. The rings are colored in orange and light yellow represent sextets and migrated sextets, respectively.

First, let us see kekulenes. The peaks colored in red in low-field region, originate from the internal protons of kekulenes structures (see the H atoms colored in red in Fig. 6(a) and (b)). The blue peaks are associated with external protons bonded in the (migrating) sextets rings. The third group of peaks colored in green falls in the upfield region, corresponding to the external protons attached to the nonsextets rings. The three groups of peaks are commonly seen in the experimental ^{1}H NMR spectra of [12]kekulene,[1,16,62] generalized kekulenes,[23] septulene,[22] octulene[8] and generalized infinitenes.[27] The H atoms colored in blue bonded in the (migrating) sextets rings are obviously deshielded by the aromatic rings in which the H atoms stay and are thus responsible for the peaks in low-field regions. Moreover, chemical shifts of the inner protons colored in red of kekulenes are further shifted to low field compared to those of the H atoms colored in blue, presumably owing to the additional deshielding effect from the neighboring benzenoid rings. As for the third group peaks colored in green falling in relatively high field region, the corresponding H atoms are bonded to nonsextet rings, which have almost no effective deshielding effect on these H atoms. In addition, we noticed that the H atoms colored in red in [9]kekulene fall in a lower field region compared with other kekulenes (see Fig. 6(a)), which may be due to the fact that these H atoms are closer to the adjacent aromatic rings and are thus subject to stronger deshielding effect.

For clarenes, the peaks colored red in low-field region, originate from the internal protons of clarene structures (see Fig. 6(c) and (d)), similar to the case of kekulenes (Fig. 6(a) and (b)). The deshielding effects from the parent aromatic ring of the H atoms and the neighboring rings make the peaks of these H atoms fall in lowest field. For external protons, almost all of them are attached to the nonaromatic rings. We distinguish two types of H atoms colored in blue and green, respectively, according to the number of the next-nearest neighbor rings of H atoms, being 0 and 1, respectively, which is different from kekulenes, because the latter do not have such a next-nearest neighbor ring. For example, Fig. 6(c) illustrates the definition of these two types of H atoms. The deshielding effect on the H atom labeled "a" mainly originates from the three rings, the parent ring (A), adjacent ring

(B), and next-nearest neighbor ring (C). On the other hand, for H atom labeld "b", only the parent ring (E) and adjacent ring (F) contribute to the deshielding effect. The deshielding effect from next-nearest neighbor ring (G) is negligible for H atom labeld "b" due to a large distance between them, which explains that the peaks corresponding to H atom colored in green fall in higher field compared to H atom colored in blue. For larger clarenes with N_{ring} $\geq$ 40, due to distorted structures caused by $\pi-\pi$ stacking, the relationship between chemical shift and type of H atoms is not obvious because the chemical environment around H atoms is relatively complex (see Fig. S11–S12 in ESI).

3.3.2 UV−vis absorption spectra for the lowest-energy isomers of kekulenes and clarenes

Since kekulenes and clarenes typically have a large π-conjugated system, we therefore simulated the UV-vis absorption spectra of the lowest-energy isomers of [9]kekulene, [20]kekulene, [42]clarene, and [60]clarene, as shown in the inset of Fig. 7 and in Fig. S15–S19 in ESI. The maximum absorption wavelength, λ_{max}, as a function of N_{ring} is plotted in Fig. 7. Among all considered kekulenes, the experimentally synthesized [12]kekulene displays a relatively high λ_{max}, 340 nm, in agreement with the experimental value (327 nm) (see Fig. S14 in ESI).[23,62] In general, the maximum absorption wavelength increases as the clarene size increases, as shown in Fig. 7. A least-squares fit shows that λ_{max} varies inversely and negatively with N_{ring} (see the dashed line in Fig. 7), which is similar to generalized infinitenes.[27] The red shift as the size of clarenes increases can be roughly understood by the fact that the gap between HOMO and LUMO decreases in larger π-conjugated systems.[82] In addition, we find that the molar extinction coefficients (ε) gradually increases as the increasing of melocular size (see Fig. S20 in ESI), probably due to the increase of transition probability as a result of the increasing number of frontier molecular orbitals as the size of the π-conjugated system grows.

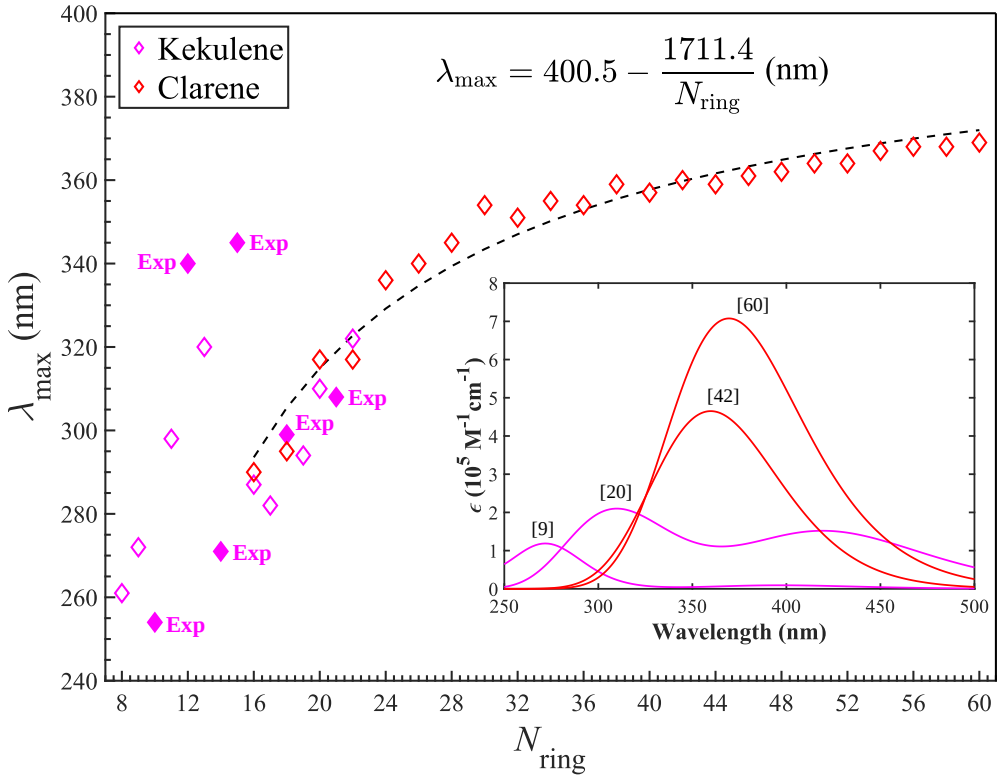

Figure 7. Maximum absorption wavelength (λ_{max}) of the simulated UV-vis spectra for the lowest-energy isomers of kekulene and clarene of various sizes, N_{ring}. The experimentally synthesized kekulenes are represented by filled symbol. The inset displays the simulated UV-vis absorption spectra for the lowest-energy isomers of kekulene and clarene with N_{ring} = 9, 20, 42, and 60.

4 Conclusion

We have systematically proposed the two novel kinds of cycloarenes, generalized kekulenes, [h_1, h_2, h_3, h_4, h_5, h_6], and clarenes, <h_1, h_2, h_3, h_4, h_5, h_6>. The generalized kekulenes have zigzag-shaped sides, while the shape of sides are in an armchair fashion for clarenes. Clarenes can have only even-numbered side lengths, while the side lengths of kekulenes can be any positive integer.

Based on the results of extensive xTB and DFT calculations, we have discovered that the relative stability of kekulene and clarene isomers is determined by π delocalization in the conjugated system by using a HMO-theory-based model. For kekulenes with long side lengths or large molecular sizes, the ground state is open-shell singlet. For smaller clarenes, we find that the number of Clar resonators can also explain the relative isomer stability more intuitively. For stadium-type clarenes, whether equiangular or nonequiangular, the molecule is flexible enough to make the two longest opposite sides of the superhexagon approach each other closely and effectively induce intramolecular $\pi-\pi$ stacking interactions, which provides a considerable additional stability. In addition, among all looped polyarenes under consideration, clarenes are almost the energetically most stable, because they achieve a maximum number of Clar sextets, which make clarenes possess a maximized π stabilization.

As we all know, $\pi-\pi$ stacking occurs widely in biological macromolecules, which plays an important role in the stability of macromolecular conformers caused by molecular flexibility. For the stadium-type clarenes, we have found two distinct conformers with a small energy difference due to the relative shift of the longest opposite sides of clarenes caused by greater flexibility of larger molecular size. Studying conformational variations caused by $\pi-\pi$ stacking will not only help improve the utilization of stacking effect, but also have far-reaching significance for the practical application of this type of looped polyarene materials.

Finally, the calculated ^{1}H NMR spectra for these new compounds show three groups of peaks corresponding to three types of H atoms in three different regions of kekulenes and clarenes. The deshielding effects from different aromatic or nonaromatic rings make H atoms

in different chemical environments have different but understandable chemical shifts. In the simulated UV-vis spectra, with the increasing size of molecules, the maximum absorption wavelength shows a red shift, reflecting a decrease in HOMO–LUMO gap. Additionally, the molar extinction coefficients (ε) also gradually increases casued by the increase of transition probability as a result of the increasing number of frontier molecular orbitals as the π-conjugated system grows. The new compounds we proposed in this work are expected to be synthesized in future synthetic efforts, and the simulated spectra will help synthetic chemists to identify these molecules in experimental characterization.

Electronic supplementary information (ESI) available

DFT refinement calculation for kekulenes and clarenes with lower xTB energies; comparison between xTB and DFT relative energies for [18]kekulenes and [48]clarenes; structural comparison between DFT and experiment for [12]kekulene; relative energies and free energies for looped polyarenes at B3LYP-D3(BJ)/6-31G*; simulated ^{1}H NMR spectra and UV-vis spectra for the lowest-energy kekulenes and clarenes; construction of equiangular and nonequiangular hexagons; comparison between HMO and DFT relative energies for representative kekulenes and clarenes; Clar resonators of [30]clarene, <2,8,2,8,2,8>; IRI maps and conformers of stadium-type clarenes; structures and Cartesian coordinates for the lowest-energy kekulenes and clarenes.

Conflicts of interest

The authors declare no conflicts of interest.

Acknowledgement

The authors acknowledge the financial support from National Natural Science Foundation of China (22073080) and Double Innovation Talent Program of Jiangsu Province (JSS-CRC2021542).

References

(1) Staab, H. A.; Diederich, F. Cycloarenes, a New Class of Aromatic Compounds, I. Synthesis of Kekulene. *Chem. Ber.* **1983**, *116*, 3487–3503.

(2) Beser, U.; Kastler, M.; Maghsoumi, A.; Wagner, M.; Castiglioni, C.; Tommasini, M.; Narita, A.; Feng, X.; Müllen, K. A C216-Nanographene Molecule with Defined Cavity as Extended Coronoid. *J. Am. Chem. Soc.* **2016**, *138*, 4322–4325.

(3) Martinez-Castro, J.; Bolat, R.; Fan, Q.; Werner, S.; Arefi, H. H.; Esat, T.; Sundermeyer, J.; Wagner, C.; Michael Gottfried, J.; Temirov, R.; Ternes, M.; Stefan Tautz, F. Disentangling the electronic structure of an adsorbed graphene nanoring by scanning tunneling microscopy. *Communications Materials* **2022**, *3*, 57.

(4) Fan, W.; Han, Y.; Dong, S.; Li, G.; Lu, X.; Wu, J. Facile Synthesis of Aryl-Substituted Cycloarenes via Bismuth(III) Triflate-Catalyzed Cyclization of Vinyl Ethers. *CCS Chem.* **2021**, *3*, 1445–1452.

(5) Buttrick, J. C.; King, B. T. Kekulenes, cycloarenes, and heterocycloarenes: addressing electronic structure and aromaticity through experiments and calculations. *Chem. Soc. Rev.* **2017**, *46*, 7–20.

(6) Majewski, M. A.; Stępień, M. Bowls, Hoops, and Saddles: Synthetic Approaches to Curved Aromatic Molecules. *Angew. Chem. Int. Ed.* **2019**, *58*, 86–116.

(7) Olea Ulloa, C.; Guajardo-Maturana, R.; Muñoz-Castro, A. On the Cation-π capabilities of infinitene (∞). Evaluation of bonding and circular dichroism properties for Infinitene-$Ag(I)_n$ (n = 1–4) complexes from relativistic DFT calculations. *Polyhedron* **2023**, *234*, 116323.

(8) Majewski, M. A.; Hong, Y.; Lis, T.; Gregoliński, J.; Chmielewski, P. J.; Cybińska, J.; Kim, D.; Stepień, M. Octulene: A Hyperbolic Molecular Belt that Binds Chloride Anions. *Angew. Chem. Int. Ed.* **2016**, *55*, 14072–14076.

(9) Banhart, F.; Kotakoski, J.; Krasheninnikov, A. V. Structural Defects in Graphene. *ACS Nano* **2011**, *5*, 26–41.

(10) Buttrick, J. C.; King, B. T. Kekulenes, cycloarenes, and heterocycloarenes: addressing electronic structure and aromaticity through experiments and calculations. *Chem. Soc. Rev.* **2017**, *46*, 7–20.

(11) Novoselov, K. S.; Fal'ko, V. I.; Colombo, L.; Gellert, P. R.; Schwab, M. G.; Kim, K. A roadmap for graphene. *Nature* **2012**, *490*, 192–200.

(12) Aihara, J.-i. π-Electron Currents Induced in Polycyclic Benzenoid Hydrocarbons and Their Relationship to Clar Structures. *J. Phys. Chem. A* **2003**, *107*, 11553–11557.

(13) Aihara, J.-i.; Makino, M. Constrained Clar Formulas of Coronoid Hydrocarbons. *J. Phys. Chem. A* **2014**, *118*, 1258–1266.

(14) Liu, C.; Ni, Y.; Lu, X.; Li, G.; Wu, J. Global Aromaticity in Macrocyclic Polyradicaloids: Hückel's Rule or Baird's Rule? *Acc. Chem. Res.* **2019**, *52*, 2309–2321.

(15) Pozo, I.; Majzik, Z.; Pavliček, N.; Melle-Franco, M.; Guitián, E.; Peña, D.; Gross, L.; Pérez, D. Revisiting Kekulene: Synthesis and Single-Molecule Imaging. *J. Am. Chem. Soc.* **2019**, *141*, 15488–15493.

(16) Diederich, F.; Staab, H. A. Benzenoid versus Annulenoid Aromaticity: Synthesis and Properties of Kekulene. *Angew. Chem. Int. Ed.* **1978**, *17*, 372–374.

(17) Krieger, C.; Diederich, F.; Schweitzer, D.; Staab, H. A. Molecular Structure and Spectroscopic Properties of Kekulene. *Angew. Chem. Int. Ed.* **1979**, *18*, 699–701.

(18) Pauling, L. The Diamagnetic Anisotropy of Aromatic Molecules. *J. Chem. Phys.* **2004**, *4*, 673–677.

(19) McWeeny, R. The Diamagnetic Anisotropy of Large Aromatic Systems: III Structures with Hexagonal Symmetry. *Proc. Phys. Soc. A* **1951**, *64*, 921.

(20) Clar, E. *The Aromatic Sextet*; Wiley: New York, 1972; pp 1–128.

(21) Haags, A. et al. Kekulene: On-Surface Synthesis, Orbital Structure, and Aromatic Stabilization. *ACS Nano* **2020**, *14*, 15766–15775, PMID: 33186031.

(22) Kumar, B.; Viboh, R. L.; Bonifacio, M. C.; Thompson, W. B.; Buttrick, J. C.; Westlake, B. C.; Kim, M.-S.; Zoellner, R. W.; Varganov, S. A.; Mörschel, P.; Teteruk, J.; Schmidt, M. U.; King, B. T. Septulene: The Heptagonal Homologue of Kekulene. *Angew. Chem. Int. Ed.* **2012**, *51*, 12795–12800.

(23) Fan, W.; Han, Y.; Wang, X.; Hou, X.; Wu, J. Expanded Kekulenes. *J. Am. Chem. Soc.* **2021**, *143*, 13908–13916.

(24) Chang, D.; Zhu, J.; Sun, Y.; Chi, K.; Qiao, Y.; Wang, T.; Zhao, Y.; Liu, Y.; Lu, X. From closed-shell edge-extended kekulenes to open-shell carbonylated cycloarene diradicaloid. *Chem. Sci.* **2023**, *14*, 6087–6094.

(25) Jia, X.; Campos-Delgado, J.; Terrones, M.; Meunier, V.; Dresselhaus, M. S. Graphene edges: a review of their fabrication and characterization. *Nanoscale* **2011**, *3*, 86–95.

(26) Bergan, J. L.; Cyvin, S. J.; Cyvin, B. N. Number of kekulé structures of single-chain corona-condensed benzenoids (cycloarenes). *Chem. Phys. Lett.* **1986**, *125*, 218–220.

(27) Du, K.; Wang, Y. Infinitenes as the Most Stable Form of Cycloarenes: The Interplay among π Delocalization, Strain, and π–π Stacking. *J. Am. Chem. Soc.* **2023**, *145*, 10763–10778.

(28) Solà, M. Forty Years of Clar's Aromatic π-Sextet Rule. *Front. Chem.* **2013**, *1*, 22.

(29) Wang, Y. Quantitative Resonance Theory Based on the Clar Sextet Model. *J. Phys. Chem. A* **2022**, *126*, 164–176.

(30) Wang, Y. The GenInfi program. 2023; `https://github.com/yangwangmadrid/GenInfi`, (accessed March 29, 2023).

(31) Grimme, S.; Bannwarth, C.; Shushkov, P. A Robust and Accurate Tight-Binding Quantum Chemical Method for Structures, Vibrational Frequencies, and Noncovalent Interactions of Large Molecular Systems Parametrized for All spd-Block Elements (Z = 1–86). *J. Chem. Theory Comput.* **2017**, *13*, 1989–2009.

(32) Bannwarth, C.; Ehlert, S.; Grimme, S. GFN2-xTB—An Accurate and Broadly Parametrized Self-Consistent Tight-Binding Quantum Chemical Method with Multipole Electrostatics and Density-Dependent Dispersion Contributions. *J. Chem. Theory Comput.* **2019**, *15*, 1652–1671.

(33) Semiempirical Extended Tight-Binding Program Package. 2020; `https://github.com/grimme-lab/xtb/tree/v6.3.3`, (accessed March 29, 2023).

(34) Bannwarth, C.; Caldeweyher, E.; Ehlert, S.; Hansen, A.; Pracht, P.; Seibert, J.; Spicher, S.; Grimme, S. Extended tight-binding quantum chemistry methods. *WIREs Comput. Mol. Sci.* **2021**, *11*, e1493.

(35) Frisch, M. J. et al. Gaussian 16 Rev. B.01. Wallingford, CT, 2016.

(36) Lee, C.; Yang, W.; Parr, R. G. Development of the Colle–Salvetti Correlation-Energy Formula Into a Functional of the Electron Density. *Phys. Rev. B* **1988**, *37*, 785–789.

(37) Becke, A. D. Density-Functional Thermochemistry. III. The Role of Exact Exchange. *J. Chem. Phys.* **1993**, *98*, 5648–5652.

(38) Grimme, S.; Ehrlich, S.; Goerigk, L. Effect of the damping function in dispersion corrected density functional theory. *J. Comput. Chem.* **2011**, *32*, 1456–1465.

(39) Chai, J.-D.; Head-Gordon, M. Long-Range Corrected Hybrid Density Functionals With Damped Atom–Atom Dispersion Corrections. *Phys. Chem. Chem. Phys.* **2008**, *10*, 6615–6620.

(40) Dunning, T. H. Gaussian basis sets for use in correlated molecular calculations. I. The atoms boron through neon and hydrogen. *J. Chem. Phys.* **1989**, *90*, 1007–1023.

(41) Cohen, A. J.; Mori-Sánchez, P.; Yang, W. Insights into Current Limitations of Density Functional Theory. *Science* **2008**, *321*, 792–794.

(42) Szczepanik, D. W.; Solà, M.; Andrzejak, M.; Pawełek, B.; Dominikowska, J.; Kukułka, M.; Dyduch, K.; Krygowski, T. M.; Szatylowicz, H. The role of the long-range exchange corrections in the description of electron delocalization in aromatic species. *J. Comput. Chem.* **2017**, *38*, 1640–1654.

(43) Grimme, S. Supramolecular Binding Thermodynamics by Dispersion-Corrected Density Functional Theory. *Chem. Eur. J.* **2012**, *18*, 9955–9964.

(44) Lu, T.; Chen, Q. Shermo: A general code for calculating molecular thermochemistry properties. *Comput. Theor. Chem.* **2021**, *1200*, 113249.

(45) Wang, Y. Extension and Quantification of the Fries Rule and Its Connection to Aromaticity: Large-Scale Validation by Wave-Function-Based Resonance Analysis. *J. Chem. Inf. Model.* **2022**, *62*, 5136–5148.

(46) Wang, Y. Superposition of Waves or Densities: Which is the Nature of Chemical Resonance? *J. Comput. Chem.* **2021**, *42*, 412–417.

(47) Wang, Y. A Reliable and Efficient Resonance Theory Based on Analysis of DFT Wave Functions. *Phys. Chem. Chem. Phys.* **2021**, *23*, 2331–2348.

(48) Wang, Y. The EzReson program. 2023; `https://github.com/yangwangmadrid/EzReson`, (accessed March 29, 2023).

(49) Lu, T.; Chen, Q. Interaction Region Indicator: A Simple Real Space Function Clearly Revealing Both Chemical Bonds and Weak Interactions. *Chem. Methods* **2021**, *1*, 231–239.

(50) Lu, T.; Chen, F. Multiwfn: A multifunctional wavefunction analyzer. *J. Comput. Chem.* **2012**, *33*, 580–592.

(51) Humphrey, W.; Dalke, A.; Schulten, K. VMD: Visual molecular dynamics. *J. Mol. Graphics* **1996**, *14*, 33–38.

(52) Marenich, A. V.; Cramer, C. J.; Truhlar, D. G. Universal Solvation Model Based on Solute Electron Density and on a Continuum Model of the Solvent Defined by the Bulk Dielectric Constant and Atomic Surface Tensions. *J. Phys. Chem. B* **2009**, *113*, 6378–6396.

(53) Krzeszewski, M.; Ito, H.; Itami, K. Infinitene: A Helically Twisted Figure-Eight [12]Circulene Topoisomer. *J. Am. Chem. Soc.* **2022**, *144*, 862–871.

(54) Fan, W.; Matsuno, T.; Han, Y.; Wang, X.; Zhou, Q.; Isobe, H.; Wu, J. Synthesis and Chiral Resolution of Twisted Carbon Nanobelts. *J. Am. Chem. Soc.* **2021**, *143*, 15924–15929.

(55) Fan, W.; Matsuno, T.; Han, Y.; Wang, X.; Zhou, Q.; Isobe, H.; Wu, J. Correction to "Synthesis and Chiral Resolution of Twisted Carbon Nanobelts". *J. Am. Chem. Soc.* **2022**, *144*, 22332.

(56) Lodewyk, M. W.; Siebert, M. R.; Tantillo, D. J. Computational Prediction of ^{1}H and ^{13}C Chemical Shifts: A Useful Tool for Natural Product, Mechanistic, and Synthetic Organic Chemistry. *Chem. Rev.* **2012**, *112*, 1839–1862.

(57) Bally, T.; Rablen, P. R. Quantum-Chemical Simulation of ^{1}H NMR Spectra. 2. Comparison of DFT-Based Procedures for Computing Proton–Proton Coupling Constants in Organic Molecules. *J. Org. Chem.* **2011**, *76*, 4818–4830.

(58) Jain, R.; Bally, T.; Rablen, P. R. Calculating Accurate Proton Chemical Shifts of Organic Molecules with Density Functional Methods and Modest Basis Sets. *J. Org. Chem.* **2009**, *74*, 4017–4023.

(59) Rablen, P. R.; Pearlman, S. A.; Finkbiner, J. A Comparison of Density Functional Methods for the Estimation of Proton Chemical Shifts with Chemical Accuracy. *J. Phys. Chem. A* **1999**, *103*, 7357–7363.

(60) Jiao, W.-H.; Xu, T.-T.; Yu, H.-B.; Chen, G.-D.; Huang, X.-J.; Yang, F.; Li, Y.-S.; Han, B.-N.; Liu, X.-Y.; Lin, H.-W. Dysideanones A–C, Unusual Sesquiterpene Quinones from the South China Sea Sponge Dysidea avara. *J. Nat. Prod.* **2014**, *77*, 346–350.

(61) Perdew, Density-functional approximation for the correlation energy of the inhomogeneous electron gas. *Phys. Rev. B* **1986**, *33 12*, 8822–8824.

(62) Staab, H. A.; Diederich, F.; Krieger, C.; Schweitzer, D. Cycloarenes, a New Class of Aromatic Compounds, II. Molecular Structure and Spectroscopic Properties of Kekulene. *Chem. Ber.* **1983**, *116*, 3504–3512.

(63) Hou, H.; Zhao, X.-J.; Tang, C.; Ju, Y.-Y.; Deng, Z.-Y.; Wang, X.-R.; Feng, L.-B.; Lin, D.-H.; Hou, X.; Narita, A.; Müllen, K.; Tan, Y.-Z. Synthesis and assembly of extended quintulene. *Nat. Commun.* **2020**, *11*, 3976.

(64) Szczepanik, D. W.; Solà, M.; Krygowski, T. M.; Szatylowicz, H.; Andrzejak, M.; Pawełek, B.; Dominikowska, J.; Kukułka, M.; Dyduch, K. Aromaticity of acenes: the model of migrating π-circuits. *Phys. Chem. Chem. Phys.* **2018**, *20*, 13430–13436.

(65) Bendikov, M.; Duong, H. M.; Starkey, K.; Houk, K. N.; Carter, E. A.; Wudl, F. Oligoacenes: Theoretical Prediction of Open-Shell Singlet Diradical Ground States. *J. Am. Chem. Soc.* **2004**, *126*, 7416–7417.

(66) Hückel, E. Quantentheoretische Beiträge zum Benzolproblem. I. Die Elektronenkonfiguration des Benzols und werwandter Verbindungen. *Z. Phys.* **1931**, *70*, 204–286.

(67) Hückel, E. Quantentheoretische Beiträge zum Bezolproblem. II. Quantentheorie der induzierten Polaritäten. *Z. Phys.* **1931**, *72*, 310–337.

(68) Hückel, E. Quantentheoretische Beiträge zum Problem der aromatischen und ungesättigten Verbindungen. III. *Z. Phys.* **1932**, *76*, 628–648.

(69) Hückel, E. Quantentheoretische Beiträge zum Bezolproblem. IV. Die freien Radikale der organischen Chemie. *Z. Phys.* **1933**, *83*, 632.

(70) Wang, Y.; Zhou, Y.; Du, K. Enumeration, Nomenclature and Stability Rules of Carbon Nanobelts. *ChemRxiv* **2023**, DOI:10.26434/chemrxiv–2023–85ww5.

(71) Esser, B.; Bandyopadhyay, A.; Rominger, F.; Gleiter, R. From Metacyclophanes to Cyclacenes: Synthesis and Properties of $[6.8]_3$Cyclacene. *Chem. Eur. J.* **2009**, *15*, 3368–3379.

(72) Nishiuchi, T.; Iyoda, M. Bent π-Conjugated Systems Composed of Three-Dimensional Benzoannulenes. *Chem. Rec.* **2015**, *15*, 329–346.

(73) Iyoda, M.; Kuwatani, Y.; Nishinaga, T.; Takase, M.; Nishiuchi, T. *Fragments of Fullerenes and Carbon Nanotubes*; John Wiley & Sons, Ltd, 2011; Chapter 12, pp 311–342.

(74) Povie, G.; Segawa, Y.; Nishihara, T.; Miyauchi, Y.; Itami, K. Synthesis of a carbon nanobelt. *Science* **2017**, *356*, 172–175.

(75) Povie, G.; Segawa, Y.; Nishihara, T.; Miyauchi, Y.; Itami, K. Synthesis and Size-Dependent Properties of [12], [16], and [24]Carbon Nanobelts. *J. Am. Chem. Soc.* **2018**, *140*, 10054–10059.

(76) Xia, Z.; Pun, S. H.; Chen, H.; Miao, Q. Synthesis of Zigzag Carbon Nanobelts through Scholl Reactions. *Angew. Chem. Int. Ed.* **2021**, *60*, 10311–10318.

(77) Cheung, K. Y.; Gui, S.; Deng, C.; Liang, H.; Xia, Z.; Liu, Z.; Chi, L.; Miao, Q. Synthesis of Armchair and Chiral Carbon Nanobelts. *Chem* **2019**, *5*, 838–847.

(78) Bergman, H. M.; Kiel, G. R.; Handford, R. C.; Liu, Y.; Tilley, T. D. Scalable, Divergent Synthesis of a High Aspect Ratio Carbon Nanobelt. *J. Am. Chem. Soc* **2021**, *143*, 8619–8624.

(79) Shi, T.-H.; Guo, Q.-H.; Tong, S.; Wang, M.-X. Toward the Synthesis of a Highly Strained Hydrocarbon Belt. *J. Am. Chem. Soc.* **2020**, *142*, 4576–4580.

(80) Zhou, Q.; Hou, X.; Wang, J.; Ni, Y.; Fan, W.; Li, Z.; Wei, X.; Li, K.; Yuan, W.; Xu, Z.; Zhu, M.; Zhao, Y.; Sun, Z.; Wu, J. A Fused [5]Helicene Dimer with a Figure-Eight Topology: Synthesis, Chiral Resolution, and Electronic Properties. *Angew. Chem. Int. Ed.* **2023**, *62*, e202302266.

(81) Funhoff, D. J. H.; Staab, H. A. Cyclo[d.e.d.e.e.d.e.d.e.e.]decakisbenzene, a New Cycloarene. *Angew. Chem. Int. Ed.* **1986**, *25*, 742–744.

(82) Iwamoto, T.; Watanabe, Y.; Sakamoto, Y.; Suzuki, T.; Yamago, S. Selective and Random Syntheses of [n]Cycloparaphenylenes (n = 8–13) and Size Dependence of Their Electronic Properties. *J. Am. Chem. Soc.* **2011**, *133*, 8354–8361.

Graphical TOC Entry